HHS Public Access

Author manuscript

J Phys Chem B. Author manuscript; available in PMC 2016 March 30.

Published in final edited form as:

J Phys Chem B. 2016 February 4; 120(4): 633–640. doi:10.1021/acs.jpcb.5b09040.

Probing the Secondary Structure of Membrane Peptides Using ^{2}H-Labeled d_{10}-Leucine via Site-Directed Spin-Labeling and Electron Spin Echo Envelope Modulation Spectroscopy

Lishan Liu, **Indra D. Sahu**, **Robert M. McCarrick**, and **Gary A. Lorigan***

Department of Chemistry and Biochemistry, Miami University, Oxford, Ohio 45056, United States

Abstract

Previously, we reported an electron spin echo envelope modulation (ESEEM) spectroscopic approach for probing the local secondary structure of membrane proteins and peptides utilizing ^{2}H isotopic labeling and site-directed spin-labeling (SDSL). In order to probe the secondary structure of a peptide sequence, an amino acid residue (i) side chain was ^{2}H-labeled, such as ^{2}H-labeled d_{10}-Leucine, and a cysteine residue was strategically placed at a subsequent nearby position (denoted as $i + 1$ to $i + 4$) to which a nitroxide spin label was attached. In order to fully access and demonstrate the feasibility of this new ESEEM approach with ^{2}H-labeled d_{10}-Leu, four Leu residues within the AChR M2δ peptide were fully mapped out using this ESEEM method. Unique ^{2}H-ESEEM patterns were observed with the ^{2}H-labeled d_{10}-Leu for the AChR M2δ α-helical model peptide. For proteins and peptides with an α-helical secondary structure, deuterium modulation can be clearly observed for $i \pm 3$ and $i \pm 4$ samples, but not for $i \pm 2$ samples. Also, a deuterium peak centered at the ^{2}H Larmor frequency of each $i \pm 4$ sample always had a significantly higher intensity than the corresponding $i + 3$ sample. This unique feature can be potentially used to distinguish an α-helix from a π-helix or 3_{10}-helix. Moreover, ^{2}H modulation depth for ESEEM samples on Leu10 were significantly enhanced which was consistent with a kinked or curved structural model of the AChR M2δ peptide as suggested by previous MD simulations and NMR experiments.

Graphical abstract

*Corresponding Author: lorigag@miamioh.edu.

Supporting Information

The Supporting Information is available free of charge on the ACS Publications website at DOI: 10.1021/acs.jpcb.5b09040. Three-pulse ESEEM experimental data of AChR M2δ with ^{2}H-labeled d_{10}-Leu at the N-terminal (−) and C-terminal (+) sides in DMPC/DHPC (3.5:1) bicelles at $\tau = 200$ ns for $i + 1$ to $i + 4$ in time domain and frequency domain (PDF)

The authors declare no competing financial interest.

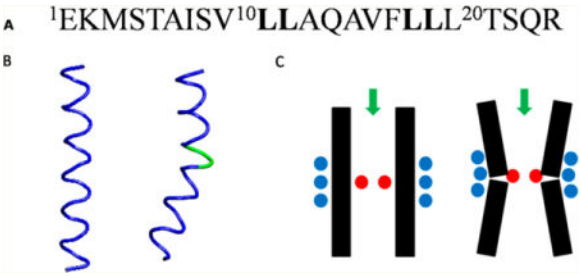

INTRODUCTION

A majority of membrane protein structural motifs fall into two categories: membrane-spanning or surface-associated α-helix or α-helix bundles and β-barrels.[1,2] More than 70% of membrane proteins with solved 3-D structures are proteins comprised of α-helices.[1] As a result of the abundance of secondary structures in membrane proteins, assembly, packing, and interaction of membrane proteins are largely affected, if not dictated by the secondary structure of membrane proteins.[3] Generally, better knowledge about the secondary structure, particularly the site-specific secondary structure, is useful toward a better understanding of membrane proteins function, dynamics, and protein—lipid interactions.[4] Also, the formation and transition of secondary structural components are crucial for a variety of cellular processes ranging from protein folding and refolding to the amyloid deposits in various neurodegenerative disorders such as Alzheimer's, Huntington's, and Parkinson's disease.[5]

There are several established biophysical techniques that are used to study secondary structures of membrane proteins such as circular dichroism, solid-state nuclear magnetic resonance (NMR), FT-Raman, and ATR FT-IR.[6–10] The Lorigan lab is developing a powerful novel ESEEM approach to probe the local secondary structure of membrane proteins that is advantageous when compared to other structural biological techniques.[11–13]ESEEM spectroscopy coupled with site-directed spin-labeling (SDSL) can provide valuable local secondary structural information (α-helix and β-strand) of membrane proteins and peptides in lipid bilayers.[13] Moreover, the high sensitivity of this ESEEM approach only requires a small amount of sample and a short amount of data acquisition time.[11] Those features make this approach extremely suitable for studying inherently difficult systems such as membrane protein systems.[14]

Figure 1 shows the SDSL and isotopic labeling scheme for this ESEEM approach on a model α-helical peptide (AChR M2δ). For this ESEEM approach, the side chain of one amino acid (such as Leu) in a model peptide at position *i* was selectively labeled with ^{2}H (blue in Figure 1). A nitroxide spin label was attached to a mutated cysteine residue on a subsequent position on each sample (denoted as *i* + 1 to *i* + 4, yellow in Figure 1) which is one, two, three, or four amino acids away from the ^{2}H-labeled Leu.[12] ESEEM spectroscopy can detect the weak dipolar coupling between the spin label and ^{2}H atoms up to 8 Å. When the ^{2}H-labeled amino acid and spin-labeled cysteine are three or four amino acids away (*i* + 3 or *i* + 4), the ^{2}H-labeled amino acid and the spin label point to the same side of the helix (Figure 1A). Thus, weak dipolar couplings between ^{2}H nuclei and the nitroxide can be detected for *i* + 3 and *i* + 4 samples. Due to the fact that a typical α-helix has 3.6 amino

acids per turn and a 5.4 Å pitch, the ^{2}H-labeled amino acid side chain and the nitroxide spin label point to opposite sides of the helix when they are one or two amino acids away (i + 1 or i + 2). As shown in Figure 1B, the distance between the ^{2}H on the amino acid side chain and the nitroxide spin label is larger than the ESEEM detection limitation. Thus, deuterium modulation would not be detected in the ESEEM time domain data or in the frequency domain data.[11–13]

Previously, we demonstrated the feasibility of this ESEEM approach using ^{2}H-labeled d_{10}-Leu and ^{2}H-labeled d_8-Val as probes.[11,12] Since ^{2}H-labeled d_{10}-Leu has been shown as a very efficient ^{2}H-labeled probe for this ESEEM approach, a more indepth understanding about its ESEEM pattern and variations at different positions could be extremely helpful for its future application in biological systems.[11] Here, we further explore the ESEEM signal pattern of an α-helix with ^{2}H-labeled d_{10}-Leu residues and provide a library of valuable data for this ^{2}H-labeled probe for the first time. Multiple ^{2}H-labeled d_{10}-Leu residues on AChR M2δ peptides were mapped out on both sides with SDSL to provide a more detailed description of the ESEEM pattern. All of the ESEEM data sets observed at different sites showed a similar distinguishing α-helical ESEEM spectra pattern. Also, modulation depth of the $i \pm 4$ sample for each set of data was larger than the corresponding $i \pm 3$ sample for ^{2}H-labeled d_{10}. This regularity can potentially be used to distinguish an α-helical structure from other less common helical structures such as 3_{10}-helix or π-helix.

EXPERIMENTAL METHODS

The M2δ peptide of the nicotinic acetylcholine receptor (AChR) with 23 amino acid residues was used as an α-helical model for transmembrane peptides and proteins (denoted as AChR M2δ).[15,16] Table 1 shows the amino acid sequences of the wild type and all experimental constructs of the M2δ peptides. For this study, four Leu residues at positions 10,11, 17, and 18 were mapped out with this ESEEM approach. Four different peptides were designed on the left (−) and the right (+) side for each Leu residue. The ^{2}H-labeled d_{10}-Leu was at position i with the cysteine (denoted as X) at four successive positions (denoted as i + 1 to i + 4).

All peptides were synthesized using Fmoc solid phase peptide synthesize chemistry on a CEM microwave solid phase peptide synthesizer.[17] A resin with a low loading (0.2 mmol/g) and a high swallow rate was chosen to increase the yield of this relatively hydrophobic peptide sequence. ^{2}H-labeled d_{10}-Leu (Isotec) was dissolved in dimethylformamide and used as the ^{2}H probe and incorporated into each peptide at a designated position (i). Those peptides were cleaved from their resin supports in a cleavage cocktail with trifluoroacetic acid/anisole/triisopropylsilane/H_2O (85%/5%/5%/5%) for 3 h. The cleavage cocktail was evaporated by N_2 gas flow until peptide precipitation started to appear. Methyl *tert*-butyl ether was added to assist the precipitation of peptide and wash off any possible residual trifluoroacetic acid. The crude peptides were dried under a vacuum overnight. Reverse-phase HPLC was used for purification with a C4 preparation column and a gradient of 5%–95% solvent B (90% acetonitrile).[18] Purified peptides were labeled with a fivefold excess of MTSL (Toronto Research Chemicals) in DMSO for 20 h, and excess MTSL was removed by HPLC. MALDI-TOF was utilized to confirm the molecular weight and the purity of

target peptides. HPLC fractions for pure and labeled peptides were lyophilized to a powder form for further usage and storage.

For these experiments, bicelles were used as a membrane mimic system to yield high-quality ESEEM data. MTSL-labeled M2δ peptides were integrated into DMPC/DHPC (3.5/1) bicelles at a 1:1000 molar ratio. X-band CW-EPR (~9 GHz) spectroscopy was used to measure spin concentrations (~150 μM) of all bicelle samples. Three-pulse ESEEM measurements were performed on a Bruker ELEXSYS E580 with an ER 4118X MS3 resonator using a 200 ns tau value with a microwave frequency of ~9.269 GHz at 80 K.[11–13] For all samples, a starting T of 386 ns and 512 points in 12 ns increments were used to collect the spectra. All ESEEM data were obtained with 40 μL of bicelle samples and 40 scans.[11,12]

The original ESEEM time domain data were fit to a two-component exponential decay.[11,12] The maximum value of the exponential fit was scaled to 1, and the same factor was applied to the time domain data. The exponential fit was then subtracted from the time domain data and yielded a scaled ESEEM spectrum with modulation about zero. A cross-term averaged Fourier transformation (FT) was performed to the resulting spectrum to generate the corresponding frequency domain with minimized dead time artifacts.[11,12] Maximum deuterium peaks intensities at 2.3 MHz were measured and recorded for further analysis.

RESULTS

Figure 2 shows three-pulse ESEEM data for ^{2}H-labeled d_{10}-Leu18 (i−1 through i−4) M2δ peptides incorporated into DMPC/DHPC (3.5/1) bicelles. In the time domain data (Figure 2 left), ^{2}H modulation is clearly observed for $i - 3$ and $i - 4$ samples of ^{2}H-labeled d_{10}-Leu18 M2δ peptides. Also, a corresponding ^{2}H peak is clearly observed for those samples centered at the ^{2}H Larmor frequency of 2.3 MHz in the frequency domain data (Figure 2 right). However, there was no ^{2}H modulation observed for the ^{2}H-labeled d_{10}-Leu11 $i - 2$ or $i - 1$ M2δ samples. These results reveal a unique ESEEM pattern for an α-helix which is consistent with previous ESEEM results.[11–13] Despite the longer side chain with more flexibility of the Leu amino acid, ESEEM spectra still revealed a similar pattern for this α-helix. At the same time, the modulation depth in the time domain data and the FT peak intensity in the frequency domain data of $i - 3$ and $i - 4$ positions were comparable to previous results.[11] The high signal-to-noise ratio of ^{2}H-labeled d_{10}-Leu makes it a very efficient side chain probe for this ESEEM technique.

ESEEM data for all eight sets of AChR M2δ samples were collected under the same sample and experimental conditions. The original time domain and frequency domain data are shown in the Supporting Information (Figures S1–S4). Normalized ^{2}H frequency domain FT peak intensities for all data sets were measured and plotted in Figure 3. Several differences were noticed depending upon the location of the ^{2}H-labeled d_{10}-Leu and the spin label. ^{2}H peak intensities for $i \pm 4$ positions varied from 0.1 to 0.6, while for $i \pm 3$ positions it varied from 0.03 to 0.3. Any frequency domain spectra with an obvious ^{2}H peak had a normalized intensity larger than 0.02 (indicted by the red line). Despise the variation of peak intensities between different data sets; it is obvious that all of them have the same pattern within each

set of $i \pm 1$ through $i \pm 4$ data as demonstrated in Figure 3A. No ^{2}H modulation was observed for any of the $i \pm 2$ samples. Most $i \pm 1$ positions did not show any modulation above the noise level. Leu11 minus 1 and Leu17 minus 1 position showed a minor ^{2}H peak near the noise level but were several folds lower than its corresponding $i \pm 3$ and $i \pm 4$ positions. Clearly, ESEEM data from all $i \pm 3$ and $i \pm 4$ positions showed significant ^{2}H modulation in the time domain and a strong ^{2}H peak in the frequency domain (see Figures S1–S4). Also, all of the data sets demonstrated high sensitivity with excellent signal-to-noise ratios with less than 2 h of total data acquisition time.

In Figure 3B, the ESEEM data are reorganized according to different positions ($i \pm x$) for comparison. The results clearly indicate that most ^{2}H peak amplitudes of $i \pm 3$ and $i \pm 4$ samples on the N-terminal side (−) were higher than the corresponding C-terminal side (+). However, the ESEEM data of the Leu10 position showed significantly larger ^{2}H FT peak amplitudes for both the N-terminal and C-terminal sides. Also, a ^{2}H FT peak for the $i - 1$ sample is observed for this Leu position.

Figure 4 compares the normalized frequency domain ^{2}H FT peak intensities of $i \pm 4$ and $i \pm 3$ positions for a particular ^{2}H-labeled d_{10}-Leu. The peak intensities of the $i \pm 4$ sample were plotted against the corresponding $i \pm 3$ sample. The red line in Figure 4 represents equal ^{2}H FT peak intensities at $i \pm 4$ and $i \pm 3$ positions, whereas the blue line is indicative of the $i \pm 4$ peak twice as large as the corresponding $i \pm 3$ peak. The graph clearly indicates that all ESEEM data from the ^{2}H-labeled d_{10}-Leu AChR M2δ peptides fell in this region, which indicated that $i \pm 4$ samples always showed a peak with at least a two-fold increase in the ^{2}H FT peak intensity rather than the corresponding $i \pm 3$ with d_{10}-Leu isotopic probe for an α-helical structure.

DISCUSSION

The nicotinic acetylcholine receptor is a ligand-gated ion channel receptor which is important for signal transduction across plasma membranes.[19] It consists of five protein subunits with each of them containing four transmembrane helices, known as M1–M4. The M2 segment is a membrane-spanning α-helix with 23 amino acid residues that is highly conserved and responsible for assembly of the channel pore. High-resolution structures of both the AChR protein and the isolated M2 segment peptide have been obtained.[16,20–22] In addition, it has been shown that the AchR M2δ peptide has a 14° tilt angle with respect to the membrane normal upon insertion into DMPC bilayers.[18,23] In previous ESEEM studies utilizing ^{2}Hlabeled d_8 and ^{2}H-labeled d_{10}-Leu as the ^{2}H probe, ESEEM data indicated that the distance between ^{2}H atoms on the amino acid side chain and the spin label are within 8 Å for $i + 3$ and $i + 4$ positions, but not for $i + 1$ or $i + 2$ positions.[11,12]

General ESEEM Pattern for α-Helix

In this research, all ESEEM data showed a similar pattern, which is indicative of an α-helical structure. Weak dipolar coupling can be detected between ^{2}H nuclei on the Leu side chain and a nitroxide spin label for $i \pm 3$ and $i \pm 4$ positions for all Leu residues on both the N-terminal (−) and the C-terminal (+) sides. Those results indicated that side chain distances between ^{2}H-labeled Leu residues and spin labels are within the 8 Å detection limit for $i \pm 3$

and $i \pm 4$ positions due to the unique 3.6 amino acids per turn feature of the α-helical structure. Only minor ^{2}H peaks around the noise level, if any, were detected for $i \pm 1$ positions. For all the constructs that had been tested with this ESEEM approach, none of them showed any ^{2}H modulation for $i \pm 2$ positions. Different conformations of MTSL and Leu might be favored due to unique side chain or tertiary interactions depending upon their environment. All of these factors play a role in the ^{2}H modulation depth and can affect the corresponding FT intensity. However, all of the ESEEM results obtained so far demonstrated that the ESEEM spectra pattern for an α-helix ($i \pm 1$ to $i \pm 4$) was not affected by the flexibility of the MTSL or the Leu side chain, which verify the reliability of this ESEEM approach on identifying secondary structural motifs.

Relative ^{2}H Peak Intensity for $i \pm 3$ and $i \pm 4$ Positions

Previous ESEEM studies have revealed a distinguishing pattern for an α-helical secondary structure with ^{2}H-labeled d_{10}-Leu and ^{2}H-labeled d_8-Val.[11,12] ^{2}H modulation can be detected for $i \pm 3$ and $i \pm 4$ positions, but not $i \pm 1$ or $i \pm 2$ positions. Beside the similar pattern that ^{2}H-labeled d_{10}-Leu and ^{2}H-labeled d_8-Val share for an α-helix, Leu demonstrated some unique features due to the longer and more flexible side chain. The $i \pm 4$ to $i \pm 3$ ratio shown in Figure 4 reveals a unique pattern for Leu in which the $i \pm 4$ positions have much larger ^{2}H peaks when compared to the corresponding $i \pm 3$ positions. Since a standard α-helix has a 3.6 amino acid per turn regularity, the angle between the side chain of the amino acid and the MTSL with respect to the helical axis was smaller in $i \pm 4$ positions than $i \pm 3$ positions.[24–26] As the side chain gets longer, the distance between the ^{2}H atoms on the Leu side chain and the nitroxide spin label reflect this angle difference more significantly. Thus, the ESSEM results always showed a larger ^{2}H FT peak when utilizing ^{2}H-labeled d_{10}-Leu as a probe. The ESEEM results indicate that the small angular difference between $i \pm 4$ and $i \pm 3$ positions of an α-helix can be detected with this ESEEM approach.

With this unique pattern of ^{2}H-labeled d_{10}-Leu, this new approach could potentially identify less abundant helical structures such as a 3_{10}-helix or a π-helix. In the case of the 3_{10}-helix, the $i \pm 3$ position should have a larger ^{2}H FT ESEEM peak than the corresponding $i \pm 4$ position due to the 3.1 amino acid per turn regularity while $i \pm 1$ and $i \pm 2$ positions should not show any ^{2}H modulation.[27] As for the π-helix, it has four amino acids per turn. Thus, the $i \pm 3$ and the $i \pm 1$ should have similar ^{2}H modulation depths, while the $i \pm 2$ would not show any modulation as a normal α-helical structure. Also, the $i \pm 4$ position should have the largest peak when compared to the corresponding $i \pm 1$ and $i \pm 3$ positions.

ESEEM ^{2}H Peak Intensity and ^{2}H-Labeled Side Chain Orientations

The ESEEM modulation depth is related to $1/r^6$, where r is the distance between nuclei on the ^{2}H-labeled side chain and the spin label. This distance varies because of multiple ^{2}H nuclei and the different conformations of both the spin label and the side chain. The MTSL spin label has three torsion angle rotations about $\chi 1$, $\chi 2$, and $\chi 3$ and two additional free torsion angle rotations about $\chi 4$ and $\chi 5$.[28] However, it can be seen in Figure 3B that all ESEEM ^{2}H FT peak amplitudes of the $i \pm 3$ and $i \pm 4$ positions on the N-terminal side (−) were larger than the corresponding C-terminal side (+), which indicated that the spin label

and ^{2}H-labeled side chain were generally closer together on the N-terminal side consistently regardless of the MTSL position ($i \pm 3$ or $i \pm 4$). Thus, it is more likely that those distances were dominated by the relative orientation of the ^{2}H-labeled Leu side chain, which was fixed for each position probed rather than the spin-labeled Cys side chain in these cases. Leu side chains have two torsion angle rotations about $\chi 1$ and $\chi 2$ and two free rotation modes about the Cγ and Cδ bonds, which correspond to two (CD_3) methyl groups.[24] Thus, different conformations of the Leu side chain might be favored due to dynamic and tertiary interactions that can affect the observed ^{2}H modulation depth.[24,26,29] The ESEEM data suggest that ^{2}H-labeled Leu side chains were orientated more toward the N-terminal side of the peptide on 10, 11, 17, and 18 positions. Previous computational simulation studies have indicated that the AChR M2δ peptide has more polar amino acids and is more flexible on the N-terminal end.[30] Thus, interactions of those polar side chains with the membrane surface and water environment outside the membrane could cause the amino acid side chains on the N-terminal end to tilt slightly toward the surface of the membrane bilayer.[31] As a consequence, it is more favorable for the Leu side chains to tilt toward the N-terminal side. Also, the kink in the peptide may play a role in this observation (see below). Additional membrane peptides will be probed to study this.

ESEEM Pattern Deviation at the Leu10 Position Is Consistent with the Kinked Model of the M2δ Peptide

The structure of the AChR M2δ peptide has been characterized via solution NMR in dodecylphosphocholine (DPC) micelles (PDB: 1A11) and by solid-state NMR in mechanically oriented 1, 2-dimyristoyl-*sn*-glycerophosphcholine (DMPC) bilayers (PDB: 1EQ8).[16] The results indicate that the M2δ peptide is a transmembrane α-helix with no obvious kink. However, it should be noted the solution NMR structure was conducted in a DPC micelle complex and not a lipid bilayer.[32] Also, mechanically aligned solid-state NMR structural studies require samples with a highly oriented lipid bilayer, which is difficult to achieve and highly lipid- or peptide-dependent.[33] In contrast to those early NMR structures, cryo-EM, molecular modeling, and magical angle spinning (MAS) solid-state NMR studies of the AChR M2δ peptide suggested the helix is kinked in the vicinity of Leu11.[22,34,35] Early mutagenesis studies and sequence comparisons suggested that Leu11 plays a key role in the gating mechanism of the AChR channel.[36]Cryo-EM and molecular modeling studies proposed the open and closed states of the AChR channel with a bending motion at this position.[22] In the closed state, the AChR M2δ segment is kinked so that the Leu11 side chain adapts a conformation to prevent the ion conduction.[37] In addition, the MAS solid-state NMR results showed peptide backbone torsion angles at positions Leu10, Leu11, and Ala12 which deviate from a classic α-helical conformation.[20]

As mentioned above, ^{2}H ESEEM peak amplitudes for the Leu10 position of M2δ peptide were enhanced on both the N-terminal (−) and the C-terminal (+) side at $i \pm 3$ and $i \pm 4$ positions when compared to all other Leu residues in this study. Also, both sides of the Leu10 $i \pm 1$ position showed ^{2}H modulation larger than the other $i \pm 1$ position on the same side. The ^{2}H FT peak intensity at the $i - 1$ position is especially significant when compared to the other $i \pm 1$ position (Figure 3B). The larger ESEEM FT intensity at the Leu10 position clearly indicates that ^{2}H atoms on the Leu side chain and spin-label are closer to each other

around Leu10 when compared to other positions. This can be explained by the structure irregularity such as a kink or curve at this site, which have been suggested by previous NMR, electron microscopy (EM), and computational simulation studies.[20,34,38] The kinked model of the AChR M2δ segment shows a slight curve around residue Leu11 (Figure 5B, right). Figure 5C illustrates the effects of the kink at Leu11 on the side chain proximities on both the inner and outer sides of the channel. The side chain of Leu11 (red dots) points toward the center of the channel, while the helix bends away from the center of the channel due to the kink. Side chains of residues such as Leu10, Ala6, and Ala14 locate in the outer side of the channel and point outward from the center of the channel (blue dots). As shown in Figure 5C, the outer side of the helix would be more crowded with side chains (right) when compared to that of the straight peptide (left). Thus, side chains of those residues located in the outer side of the channel would be closer to each other due to the kink. As a result, closer distances between Leu10 side chain and MTSL at Ala6 (Leu10 $i - 4$) and Ala14 (Leu10 $i + 4$) positions, which are indicated by enhanced ESEEM ^{2}H FT peaks, were observed. Larger ESEEM ^{2}H FT peaks observed for Leu10 position samples are consistent with previously reported kinked model of AChR M2δ peptide.[20,34,38]

CONCLUSIONS

In this study, ^{2}H-labeled d_{10}-Leu has been shown to be a very powerful secondary structural probe with high sensitivity and an excellent signal-to-noise ratio to study the local α-helical secondary structure. The ESEEM data from four different Leu residues on the AChR M2δ peptide further validates this structural biology approach and provides researchers with a reference to probe α-helical secondary structural components for proteins and peptides. Moreover, the ratio of ^{2}H FT peak intensities between the $i \pm 4$ and the $i \pm 3$ samples can be potentially utilized to determine less predominant helical structures such as a 3_{10}-helix and a π-helix. Further studies need to be conducted to explore the application of this ESEEM approach to identify and distinguish more secondary structures and structural motifs. Also, different ^{2}H-labeled amino acids with different numbers of ^{2}H atoms, side chain length, and rigidity should be studied with this ESEEM approach to establish ESEEM patterns for different secondary structures. Due to the presence of multiple ^{2}H atoms on the probe and side chain flexibility, it is still difficult to obtain quantitative distance information. However, with ^{2}H-labeled side chains with less ^{2}H atoms and more rigid spin labels such as tetrathiatriarylmethyl (TAM), 2,2,6,6-tetramethylpiperidine-1-oxyl-4-amino-4-carboxylic acid (TOAC) and bifunctional spin label (BSL), more quantitative distance information can be obtained.[39,40]

This ESEEM method uses SDSL and selective deuterium labels, both of which can be incorporated into standard expression systems using site-directed mutagenesis and selective isotopic labeling techniques for applications to larger protein systems. Thus, this new ESEEM secondary structure approach can be applied to a wide variety of different protein systems that are not amiable to other biophysical techniques.

Supplementary Material

Refer to Web version on PubMed Central for supplementary material.

Acknowledgments

This work was generously supported by National Institutes of Health Grant R01 GM108026 and by the National Science Foundation Grant CHE-1305664. The pulsed EPR spectrometer was purchased through the NSF and the Ohio Board of Regents grants (MRI-0722403).

References

1. McLuskey K, Roszak AW, Zhu Y, Isaacs NW. Crystal Structures of All-Alpha Type Membrane Proteins. Eur Biophys J. 2010; 39:723–755. [PubMed: 19826804]
2. Lomize MA, Lomize AL, Pogozheva ID, Mosberg HI. OPM: Orientations of Proteins in Membranes Database. Bioinformatics. 2006; 22:623–625. [PubMed: 16397007]
3. Kurochkina N. Helix-Helix Interactions and Their Impact on Protein Motifs and Assemblies. J Theor Biol. 2010; 264:585–592. [PubMed: 20202472]
4. Bordag N, Keller S. Alpha-Helical Transmembrane Peptides: A "Divide and Conquer"" Approach to Membrane Proteins. Chem Phys Lipids. 2010; 163:1–26. [PubMed: 19682979]
5. Gross M. Proteins That Convert from Alpha Helix to Beta Sheet: Implications for Folding and Disease. Curr Protein Pept Sci. 2000; 1:339–347. [PubMed: 12369904]
6. Whitmore L, Wallace BA. Protein Secondary Structure Snalyses from Circular Dichroism Spectroscopy: Methods and Reference Databases. Biopolymers. 2008; 89:392–400. [PubMed: 17896349]
7. Greenfield NJ. Using Circular Dichroism Spectra To Estimate Protein Secondary Structure. Nat Protoc. 2006; 1:2876–2890. [PubMed: 17406547]
8. Yu X, Lorigan GA. Secondary Structure, Backbone Dynamics, and Structural Topology of Phospholamban and Its Phosphorylated and Arg9cys-Mutated Forms in Phospholipid Bilayers Utilizing 13C and 15N Solid-State NNR Spectroscopy. J Phys Chem B. 2014; 118:2124–2133. [PubMed: 24511878]
9. Roach CA, Simpson JV, JiJi RD. Evolution of Quantitative Methods in Protein Secondary Structure Determination via Deep-Ultraviolet Resonance Raman Spectroscopy. Analyst. 2012; 137:555–562. [PubMed: 22146490]
10. Carbonaro M, Nucara A. Secondary Structure of Food Proteins by Fourier Transform Spectroscopy in the Mid-Infrared Region. Amino Acids. 2010; 38:679–690. [PubMed: 19350368]
11. Liu L, Sahu ID, Mayo DJ, McCarrick RM, Troxel K, Zhou A, Shockley E, Lorigan GA. Enhancement of Electron Spin Echo Envelope Modulation Spectroscopic Methods To Investigate the Secondary Structure of Membrane Proteins. J Phys Chem B. 2012; 116:11041–11045. [PubMed: 22908896]
12. Mayo D, Zhou A, Sahu I, McCarrick R, Walton P, Ring A, Troxel K, Coey A, Hawn J, Emwas AH, Lorigan GA. Probing the Structure of Membrane Proteins with Electron Spin Echo Envelope Modulation Spectroscopy. Protein Sci. 2011; 20:1100–1104. [PubMed: 21563228]
13. Zhou A, Abu-Baker S, Sahu ID, Liu L, McCarrick RM, Dabney-Smith C, Lorigan GA. Determining α-Helical and β-Sheet Secondary Structures via Pulsed Electron Spin Resonance Spectroscopy. Biochemistry. 2012; 51:7417–7419. [PubMed: 22966895]
14. Klare JP, Steinhoff HJ. Spin Labeling EPR. Photosynth Res. 2009; 102:377–390. [PubMed: 19728138]
15. Oblatt-Montal M, Bühler LK, Iwamoto T, Tomich JM, Montal M. Synthetic Peptides and Four-Helix Bundle Proteins as Model Systems for the Pore-Forming Structure of Channel Proteins. I. Transmembrane Segment M2 of the Nicotinic Cholinergic Receptor Channel Is a Key Pore-Lining Structure. J Biol Chem. 1993; 268:14601–14607. [PubMed: 7686900]
16. Opella SJ, Marassi FM, Gesell JJ, Valente AP, Kim Y, Oblatt-Montal M, Montal M. Structures of the M2 Channel-Lining Segments from Nicotinic Acetylcholine and NMDA Receptors by NMR Spectroscopy. Nat Struct Biol. 1999; 6:374–379. [PubMed: 10201407]
17. Chandrudu S, Simerska P, Toth I. Chemical Methods for Peptide and Protein Production. Molecules. 2013; 18:4373–4388. [PubMed: 23584057]

18. Mayo DJ, Inbaraj JJ, Subbaraman N, Grosser SM, Chan CA, Lorigan GA. Comparing the Structural Topology of Integral and Peripheral Membrane Proteins Utilizing Electron Paramagnetic Resonance Spectroscopy. J Am Chem Soc. 2008; 130:9656–9657. [PubMed: 18598031]
19. Itier V, Bertrand D. Neuronal Nicotinic Receptors: from Protein Structure to Function. FEBS Lett. 2001; 504:118–125. [PubMed: 11532443]
20. Long JR, Mills FD, Raucci F. A High Resolution Structure of the Putative Hinge Region in M2 Channel-Lining Segments of the Nicotinic Acetylcholine Receptor. Biochim Biophys Acta Biomembr. 2007; 1768:2961–2970.
21. Sankararamakrishnan R, Sansom MS. Structural Features of Isolated M2 Helices of Nicotinic Receptors: Simulated Annealing via Molecular Dynamics Studies. Biophys Chem. 1995; 55:215–230. [PubMed: 7626742]
22. Unwin N. Acetylcholine Receptor Channel Imaged in the Open State. Nature. 1995; 373:37–43. [PubMed: 7800037]
23. Newstadt JP, Mayo DJ, Inbaraj JJ, Subbaraman N, Lorigan GA. Determining the Helical Tilt of Membrane Peptides Using Electron Paramagnetic Resonance Spectroscopy. J Magn Reson. 2009; 198:1–7. [PubMed: 19254856]
24. Batchelder LS, Sullivan CE, Jelinski LW, Torchia DA. Characterization of Leucine Side-Chain Reorientation in Collagen-Fibrils by Solid-State ^{2}H NMR. Proc Natl Acad Sci USA. 1982; 79:386–389. [PubMed: 6952191]
25. Columbus L, Kalái T, Jekö J, Hideg K, Hubbell WL. Molecular Motion of Spin Labeled Side Chains in Alpha-Helices: Analysis by Variation of Side Chain Structure. Biochemistry. 2001; 40:3828–3846. [PubMed: 11300763]
26. Mulder FA. Leucine Side-Chain Conformation and Dynamics in Proteins from 13C NMR Chemical Shifts. ChemBioChem. 2009; 10:1477–1479. [PubMed: 19466705]
27. Kubota T, Lacroix JJ, Bezanilla F, Correa AM. Probing α-3(10) Transitions in a Voltage-Sensing S4 Helix. Biophys J. 2014; 107:1117–1128. [PubMed: 25185547]
28. Beier C, Steinhoff HJ. A Structure-Based Simulation Approach for Electron Paramagnetic Resonance Spectra Using Molecular and Stochastic Dynamics Simulations. Biophys J. 2006; 91:2647–2664. [PubMed: 16844740]
29. Wand AJ. Dynamic Activation of Protein Function: A View Emerging from NMR Spectroscopy. Nat Struct Biol. 2001; 8:926–931. [PubMed: 11685236]
30. Kessel A, Shental-Bechor D, Haliloglu T, Ben-Tal N. Interactions of Hydrophobic Peptides with Lipid Bilayers: Monte Carlo Simulations with M2delta. Biophys J. 2003; 85:3431–3444. [PubMed: 14645040]
31. Kessel A, Haliloglu T, Ben-Tal N. Interactions of the M2delta Segment of the Acetylcholine Receptor with Lipid Bilayers: A Continuum-Solvent Model Study. Biophys J. 2003; 85:3687–3695. [PubMed: 14645060]
32. Altenbach C, Greenhalgh DA, Khorana HG, Hubbell WL. A Collision Gradient Method To Determine the Immersion Depth of Nitroxides in Lipid bilayers: Application to Spin-Labeled Mutants of Bacteriorhodopsin. Proc Natl Acad Sci USA. 1994; 91:1667–1671. [PubMed: 8127863]
33. Byström T, Strandberg E, Kovacs FA, Cross TA, Lindblom G. Influence of Transmembrane Peptides on Bilayers of Phosphatidylcholines with Different Acyl Chain Lengths Studied by Solid-State NMR. Biochim Biophys Acta Biomembr. 2000; 1509:335–345.
34. Sankararamakrishnan R, Adcock C, Sansom MS. The Pore Domain of the Nicotinic Acetylcholine Receptor: Molecular Modeling, Pore Dimensions, and Electrostatics. Biophys J. 1996; 71:1659–1671. [PubMed: 8889144]
35. Hung A, Tai K, Sansom MS. Molecular Dynamics Simulation of the M2 Helices within the Nicotinic Acetylcholine Receptor Transmembrane Domain: Structure and Collective Motions. Biophys J. 2005; 88:3321–3333. [PubMed: 15722430]
36. Galzi JL, Devillers-Thiéry A, Hussy N, Bertrand S, Changeux JP, Bertrand D. Mutations in the Channel Domain of a Neuronal Nicotinic Receptor Convert Ion Selectivity from Cationic to Anionic. Nature. 1992; 359:500–505. [PubMed: 1383829]

37. Unwin N. Refined Structure of the Nicotinic Acetylcholine Receptor at 4A Resolution. J Mol Biol. 2005; 346:967–989. [PubMed: 15701510]

38. Tikhonov DB, Zhorov BS. Kinked-Helices Model of the Nicotinic Acetylcholine Receptor Ion Channel and Its Complexes with Blockers: Simulation by the Monte Carlo Minimization Method. Biophys J. 1998; 74:242–255. [PubMed: 9449326]

39. Fielding JA, Concilio MG, Heaven G, Hollas MA. New Developments in Spin Labels for Pulsed Dipolar EPR. Molecules. 2014; 19:16998–17025. [PubMed: 25342554]

40. Sahu ID, McCarrick RM, Troxel KR, Zhang R, Smith JH, Dunagan MM, Swartz MS, Rajan PV, Kroncke BM, Sanders CR, Lorigan GA. DEER EPR Measurement for Membrane Protein Structures via Bifunctional Spin Labels and Lipodisq Nanoparticles. Biochemistry. 2013; 52:6627–6632. [PubMed: 23984855]

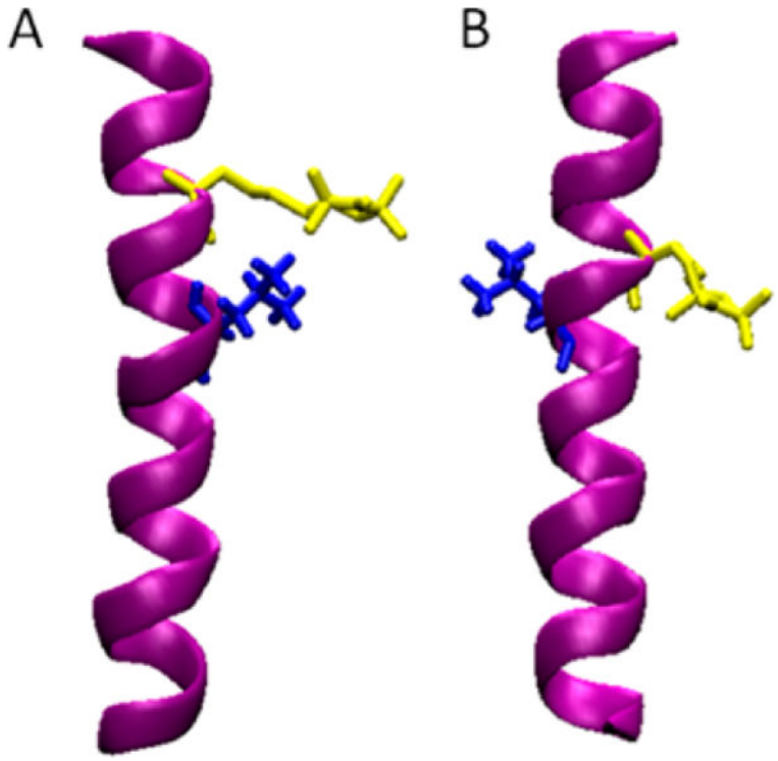

Figure 1.

ESEEM experiment SDSL and isotopic label paradigm with a model α-helix (AChR M2δ peptide in purple) for (A) the $i \pm 3$ sample and (B) the $i \pm 2$ sample. ^{2}H-labeled d_{10}-Leu residue is in blue at the 10 position. The Cys residue attached with MTSL is in yellow.

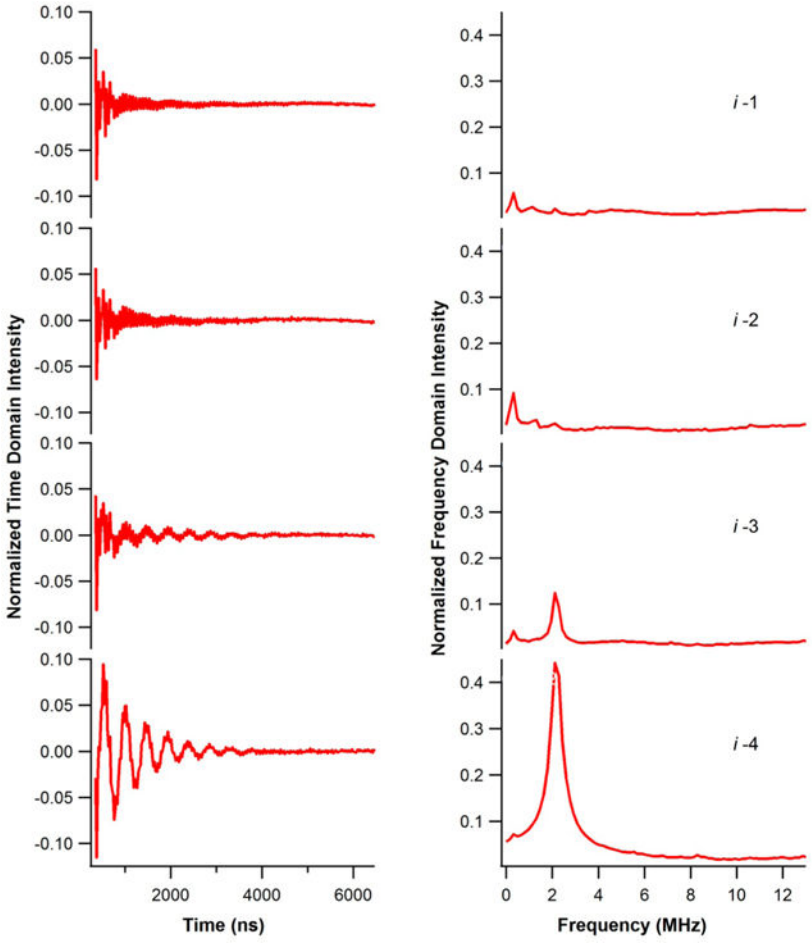

Figure 2.

Three-pulse ESEEM experimental data of AChR M2δ with ^{2}H-labeled d_{10}-Leu18 at the N-terminal (−) side in DMPC/DHPC (3.5:1) bicelles at τ = 200 ns for i + 1 to i + 4 in the time domain (left) and the frequency domain (right).

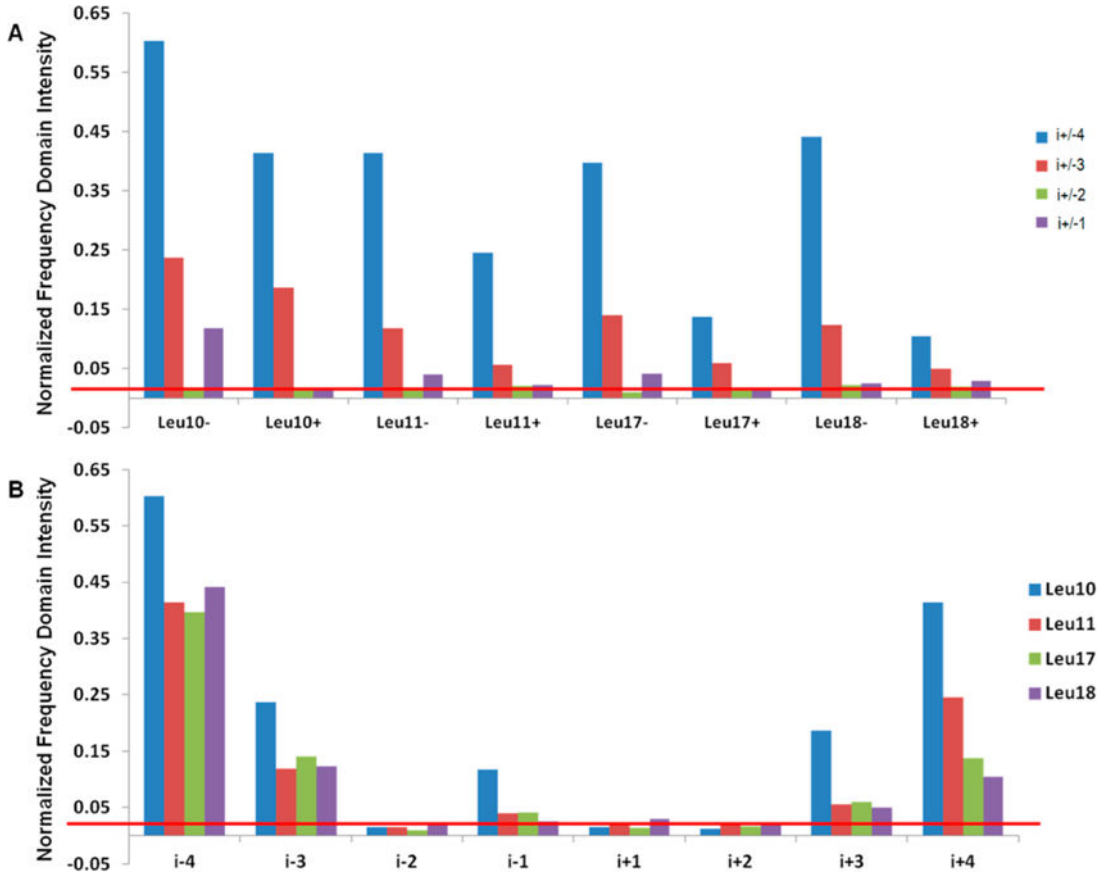

Figure 3.

Normalized ESEEM FT domain intensity from all four ^{2}H-labeled d_{10}-Leu data sets. (A) ESEEM data for each position was grouped together to demonstrate the ESEEM pattern observed for different ^{2}H-labeled residues of an α-helix. (B) The same data was rearranged for visualizing the ^{2}H peak intensity variation from $i - 4$ to $i + 4$.

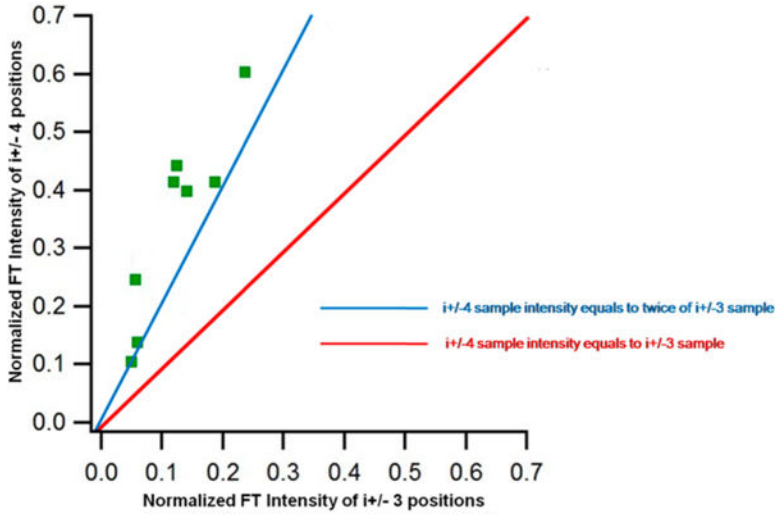

Figure 4.

Frequency domain ^{2}H peak intensity comparison between $i \pm 4$ positions and $i \pm 3$ positions for all ESEEM data. Red line represents that the ESEEM ^{2}H FT peak intensity of the $i \pm 4$ is equal to the corresponding $i \pm 3$ sample. Blue line represents that the ESEEM ^{2}H FT peak intensity of the $i \pm 4$ sample is as twice that of the corresponding $i \pm 3$ sample.

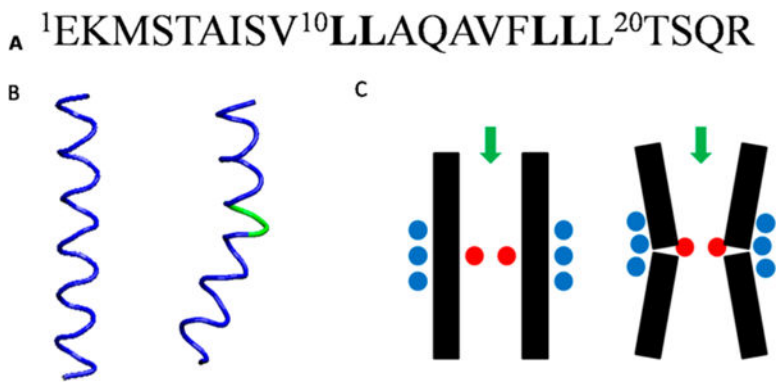

Figure 5.

(A) AChR M2δ peptide sequence with Leu residues highlighted in bold. (B) Structural representations of the straight (left) and the kinked (right) M2δ peptides. (C) Structural representations of the AChR channel with straight (left) and kinked (right) M2δ peptides. Green arrows point toward the inside of the channel. Leu11 is represented by red dots, while Ala6, Leu10, and Ala14 are shown as blue dots.

Table 1

Peptide Sequences of Wild Type AChR M2δ and ESEEM Experimental Constructs[a]

	N-terminal (−)	C-terminal (+)
wild type	**NH_2-EKMSTAISVLLAQAVFLLLTSQR-COOH**	
Leu10	NH_2-EKMSTAISXiLAQAVFLLLTSQR-COOH	NH_2-EKMSTAISViXAQAVFLLLTSQR-COOH
	NH_2-EKMSTAIXViLAQAVFLLLTSQR-COOH	NH_2-EKMSTAISViLXQAVFLLLTSQR-COOH
	NH_2-EKMSTAXSViLAQAVFLLLTSQR-COOH	NH_2-EKMSTAISViLAXAVFLLLTSQR-COOH
	NH_2-EKMSTXISViLAQAVFLLLTSQR-COOH	NH_2-EKMSTAISViLAQXVFLLLTSQR-COOH
Leu11	NH_2-EKMSTAISVXiAQAVFLLLTSQR-COOH	NH_2-EKMSTAISVLiXQAVFLLLTSQR-COOH
	NH_2-EKMSTAISXLiAQAVFLLLTSQR-COOH	NH_2-EKMSTAISVLiAXAVFLLLTSQR-COOH
	NH_2-EKMSTAIXVLiAQAVFLLLTSQR-COOH	NH_2-EKMSTAISVLiAQXVFLLLTSQR-COOH
	NH_2-EKMSTAXSVLiAQAVFLLLTSQR-COOH	NH_2-EKMSTAISVLiAQAXFLLLTSQR-COOH
Leu17	NH_2-EKMSTAISVLLAQAVXiLLTSQR-COOH	NH_2-EKMSTAISVLLAQAVFiXLTSQR-COOH
	NH_2-EKMSTAISVLLAQAXFiLLTSQR-COOH	NH_2-EKMSTAISVLLAQAVFiLXTSQR-COOH
	NH_2-EKMSTAISVLLAQXVFiLLTSQR-COOH	NH_2-EKMSTAISVLLAQAVFiLLXSQR-COOH
	NH_2-EKMSTAISVLLAXAVFiLLTSQR-COOH	NH_2-EKMSTAISVLLAQAVFiLLTXQR-COOH
Leu18	NH_2-EKMSTAISVLLAQAVFXiLTSQR-COOH	NH_2-EKMSTAISVLLAQAVFLiXTSQR-COOH
	NH_2-EKMSTAISVLLAQAVXLiLTSQR-COOH	NH_2-EKMSTAISVLLAQAVFLiLXSQR-COOH
	NH_2-EKMSTAISVLLAQAXFLiLTSQR-COOH	NH_2-EKMSTAISVLLAQAVFLiLTXQR-COOH
	NH_2-EKMSTAISVLLAQXVFLiLTSQR-COOH	NH_2-EKMSTAISVLLAQAVFLiLTSXR-COOH

[a] Wild type and experimental constructs of AChR M2δ (α-helix) are listed in this table. i is the positions where ^{2}H-labeled d_{10}-Leu was placed. X is the position for MTSL incorporation.